

Article

Influence of Silsesquioxane-Containing Ultra-Thin Polymer Films on Metal Oxide Gas Sensor Performance for the Tunable Detection of Biomarkers

Oleg Lupan ^{1,2,3,4,*}, Mihai Brinza ³, Julia Piehl ¹, Nicolai Ababii ³, Nicolae Magariu ³, Lukas Zimoch ², Thomas Strunskus ¹, Thierry Pauporte ⁴, Rainer Adelung ², Franz Faupel ¹ and Stefan Schröder ^{1,*}

¹ Chair for Multicomponent Materials, Department of Materials Science, Kiel University, Kaiserstraße 2, D-24143 Kiel, Germany; julp@tf.uni-kiel.de (J.P.); ts@tf.uni-kiel.de (T.S.); ff@tf.uni-kiel.de (F.F.)

² Functional Nanomaterials, Faculty of Engineering, Institute for Materials Science, Kiel University, Kaiserstraße 2, D-24143 Kiel, Germany; luzi@tf.uni-kiel.de (L.Z.); ra@tf.uni-kiel.de (R.A.)

³ Center for Nanotechnology and Nanosensors, Department of Microelectronics and Biomedical Engineering, Technical University of Moldova, 168 Stefan cel Mare Av., MD-2004 Chisinau, Moldova; mihai.brinza@mib.utm.md (M.B.); nicolai.ababii@mib.utm.md (N.A.); nicolae.magariu@mib.utm.md (N.M.)

⁴ Institut de Recherche de Chimie Paris-IRCP, Chimie ParisTech, PSL Université, rue Pierre et Marie Curie 11, 75231 Paris, CEDEX 05, France; thierry.pauporte@chimieparistech.psl.eu

* Correspondence: oleg.lupan@mib.utm.md (O.L.); ssch@tf.uni-kiel.de (S.S.)

Abstract: Certain biomarkers in exhaled breath are indicators of diseases in the human body. The non-invasive detection of such biomarkers in human breath increases the demand for simple and cost-effective gas sensors to replace state-of-the-art gas chromatography (GC) machines. The use of metal oxide (MOX) gas sensors based on thin-film structures solves the current limitations of breath detectors. However, the response at high humidity levels, i.e., in the case of exhaled human breath, significantly decreases the sensitivity of MOX sensors, making it difficult to detect small traces of biomarkers. We have introduced, in previous work, the concept of a hybrid gas sensor, in which thin-film-based MOX gas sensors are combined with an ultra-thin (20–30 nm) polymer top layer deposited by solvent-free initiated chemical vapor deposition (iCVD). The hydrophobic top layer enables sensor measurement in high-humidity conditions as well as the precise tuning of selectivity and sensitivity. In this paper, we present a way to increase the hydrogen (H₂) sensitivity of hybrid sensors through chemical modification of the polymer top layer. A poly(1,3,5,7-tetramethyl-tetravinylcyclotetrasiloxane) (PV4D4) thin film, already applied in one of our previous studies, is transformed into a silsesquioxane-containing top layer by a simple heating step. The transformation results in a significant increase in the gas response for H₂ ~709% at an operating temperature of 350 °C, which we investigate based on the underlying sensing mechanism. These results reveal new pathways in the biomedical application field for the analysis of exhaled breath, where H₂ indicates gastrointestinal diseases.

Keywords: sensors; tuning; hydrogen; PV4D4 polymer; silsesquioxane cage; functionalized; breath



Citation: Lupan, O.; Brinza, M.; Piehl, J.; Ababii, N.; Magariu, N.; Zimoch, L.; Strunskus, T.; Pauporte, T.; Adelung, R.; Faupel, F.; et al. Influence of Silsesquioxane-Containing Ultra-Thin Polymer Films on Metal Oxide Gas Sensor Performance for the Tunable Detection of Biomarkers. *Chemosensors* **2024**, *12*, 76. <https://doi.org/10.3390/chemosensors12050076>

Received: 29 February 2024

Revised: 16 April 2024

Accepted: 29 April 2024

Published: 5 May 2024



Copyright: © 2024 by the authors. Licensee MDPI, Basel, Switzerland. This article is an open access article distributed under the terms and conditions of the Creative Commons Attribution (CC BY) license (<https://creativecommons.org/licenses/by/4.0/>).

1. Introduction

Certain molecules in exhaled breath are biomarkers and indicators of diseases. Recent analyses and studies have concluded that all humans generate a unique profile of volatile organic compounds (VOCs) in exhaled breath, which is a product of different metabolic activities in the human body [1–3]. Thus, any change in the VOC profile has the potential to confirm a particular disease. Consequently, their detection has attracted much interest in biomedical research. A non-invasive method is desired, allowing for a simple and cost-effective analysis of exhaled breath. As stated in various papers, at this time, non-invasive diagnostic methods such as gas chromatography/mass spectrometry (GC/MS) are

considered to be the most accurate methods for obtaining a painlessly collected, extremely simple and non-invasive human breath sample [1,4].

However, this method faces many limitations due to its high cost requirements, including skilled technicians, the cost of GC/MS itself and the time required to analyze a sample. One approach to address these challenges is the development of metal oxide (MOX)-based gas sensors, which are capable of detecting low concentrations of various biomarkers/gases in human breath. More and more research studies are emerging in this direction. Recently, Lijuan Fu et al. reported a $\text{Co}_3\text{O}_4/\text{TiO}_2$ core-shell with high performance for the biomarker acetone [5]. In another study, Aasi et al. investigated atomically thin MoS_2 decorated with Pt or Pd as a promising material for colorectal cancer detection [6]. A recent review provides a comprehensive summary of the different biomarkers and the respective metal-organic frameworks applied for their detection [2]. One way to improve MOX sensors is to deposit different polymers on top of the sensors and anneal them at different temperatures to increase their properties, such as sensitivity and selectivity. A recent study presented a Cu-S semiconductor nanocomposite coated with a polyaniline nanocomposite applied for H_2S sensing [7]. As a result, it was concluded that the mechanism for improved sensing performance may be attributed to conductive composite networks. Another study obtained a Sb_2Te_3 sensor with polystyrene which resulted in good results for hydrogen sensing [8]. Some researches went further and demonstrated a wearable ethanol-sensing structure based on $\text{Ti}_3\text{C}_2\text{T}_x$ followed by functionalization using pyrrole on a disposable face mask [9]. In addition, it was demonstrated that different noble metals have an impact on different properties of TiO_2 based MOX sensors [10]. A recent review [11] mentioned that surface functionalization with different noble metal nanoparticles (NPs) improves different parameters, such as selectivity and sensitivity, as well as lowering the operation temperature and increasing long-term stability. Another recent study based on the structure-doping method [12], i.e., the use of Ag to dope an intrinsic graphdiyne with the purpose to detect SF_6 decomposition gas (HF , H_2S , SO_2 , SOF_2 , SO_2F_2), showed that the energy gap of the system was significantly decreased and the electrical conductivity was significantly improved after Ag doping. While mainly Ag and Pt seem to be used as catalysts for H_2 detection, there are also different studies that prove that there is no limit to the use of these metals for doping or functionalization with the purpose of enhancing different properties. For instance, Bi et al. [13] conducted a study on $\alpha\text{-Fe}_2\text{O}_3$ functionalized with Ag-Pt. It showed a rapid response for triethylamine vapor sensing. Thus, a lot of practical trends can be explored. One of them is enoses. Enoses, usually made from an array of sensors [14], are intended to be used as odor detectors. Some researchers use noble-metal-sensitized SnO_2/RGO as enoses for H_2 , H_2S and NO_2 [15], while others develop gas recognition models for the artificial olfactory system with gas sensor arrays [16]. In some reviews [17,18], the intention to use enoses is similar to the aim in this paper: they want to obtain a new method for non-invasive disease prediction based on different biomarkers. In some cases, even if good results are recorded, the sensor operation depends on temperature and therefore has to work at a higher operating temperature [19]. H_2 , mainly because it is easily detected by MOX sensors, is a common target in this type of application and is being researched in the industry [10,20–27]. Furthermore, it is associated with different types of gastric diseases mentioned in [4] and described in more detail in a previous work [28]. Recently, it has also been associated with the possible up regulation of neurotransmitters involved in appetite stimulation, leading to hunger suppression and weight loss [29].

In this work, we present a new addition to hybrid gas sensors, which were reported in previous studies [4,10,30], to increase their response to H_2 . A hybrid gas sensor consists of a MOX gas sensor coated with an ultrathin (~20–30 nm) polymer thin film on top of the sensor. This enables measurements in high humidity environments, which was always a problem related with conventional MOX gas sensors, as well as tuning of the sensor selectivity and performance [31,32]. High humidity levels are also encountered in exhaled breath. Hybrid sensors can circumvent this due to their hydrophobic character and enable the detection of biomarkers [6]. The polymer thin film is deposited via solvent-free

initiated chemical vapor deposition (iCVD) [33]. This allows the conformal coating of complex MOX sensor structures with a polymer film, which can be tailored by deposition parameters and precursors. The basic reaction mechanism is free-radical polymerization. The transport of gas molecules through the polymer film is accompanied by the molecular characteristics and free volume in the layer. These results motivated us to further study the compatibility of hybrid sensors for biomarker detection in exhaled human breath to further tune selectivity. We investigate in this study the influence and transport of gas molecules through an ultra-thin polymer film containing silsesquioxane cage-like structures, which should provide a different free volume compared to the cyclotetrasiloxane rings in our previous study, using poly(1,3,5,7-tetramethyl-tetravinylcyclotetrasiloxane) (PV4D4) as the top layer. The silsesquioxane structures are obtained by the heat treatment of thin films of PV4D4 deposited by iCVD in oxygen, similar to the route reported by Trujillo et al. for the formation of low-k dielectrics [34].

2. Materials and Methods

2.1. Sample Preparation

The principle behind the hybrid gas sensors investigated in this study is similar to the one described in our previous work [4,32]. We coat MOX gas sensors with a polymer thin film to protect it from moisture and to tailor the selectivity of the gas sensor. For this purpose, in this study, a 30 nm TiO₂ nanocrystalline film-based MOX sensor [10,35] was initially deposited on a glass substrate and thermally annealed at 610 °C for 60 min in air. In order to increase their performance, we furthermore functionalized the MOX sensors with Ag-Pt bimetallic NPs to increase the sensor properties, as mentioned in the Introduction. The deposition of metallic NPs onto the TiO₂ thin film was accomplished using NP beam deposition in a Haberland-type gas aggregation source. To obtain bimetallic Ag-Pt NPs, a custom-made multicomponent target, consisting of a 1 mm Pt wire embedded into a 2" Ag target was applied. Full details on the gas phase synthesis of bimetallic NPs from multicomponent targets [36] and on the surface decoration of metal oxide sensors with bimetallic AgPt NPs [37] can be found elsewhere.

In a subsequent step, the samples were coated with a PV4D4 polymer thin film. The polymer films were deposited via iCVD on the MOX sensor samples in a custom-built iCVD reactor, reported elsewhere [31,32,38]. The films were deposited in continuous flow mode using a vapor mixture of 0.3 sccm V4D4 monomer and 1 sccm tert-butyl peroxide (TBPO) initiator. The vapor flows were delivered via low-flow metering valves to the reactor [32]. A process pressure of 40 Pa was controlled by a butterfly valve (MKS instruments, Andover, MA, USA), which received feedback from a capacitive manometer (MKS Baratron, MKS instruments, Andover, MA, USA) connected to the reactor. The sample stage was cooled to 37.5 °C by backside water-cooling by a cooling bath thermostat (Huber Unichiller 007-MPC, Huber Temperiertechnik, Offenburg, Germany). The deposition process was started by resistively heating a NiCr filament array located above the cooled substrate stage with a power supply (EA PS 9036-80, EA Elektro-Automatik, Viersen, Germany) at a power of 50 W. Figure 1 illustrates the fabricated hybrid sensors used in this study.

We fabricated two sets of samples. Both hybrid sensor types were produced according to the description given above. However, one set of samples was heated to 450 °C for 30 min in ambient air in order to transform the cyclotetrasiloxane rings in the PV4D4 film into silsesquioxane cage structures, as reported by Trujillo et al. [16]. The hybrid sensors containing non-annealed PV4D4 layer are referred to as the ring layer. The hybrid sensors which were annealed contained a transformed PV4D4 layer and are referred to as the cage layer, due to the presence of silsesquioxane cage structures after the thermal annealing step.

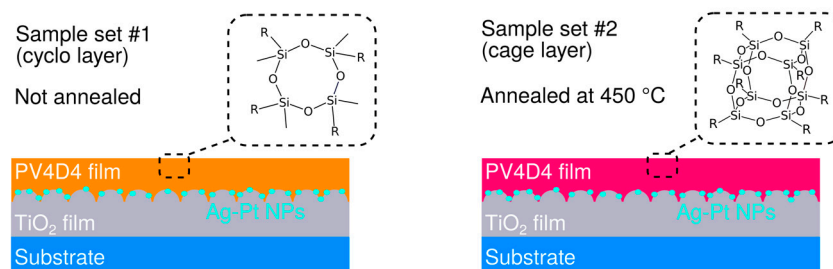


Figure 1. Illustration of the two sample sets investigated in this study. In sample set #1 the hybrid sensors, in the end, are not annealed and the PV4D4 film contains cyclotetrasiloxane rings (ring layer). In sample set #2 the hybrid sensor is annealed at 450 °C for 30 min in ambient air in order to transform the cyclotetrasiloxane rings into silsesquioxane cage structures (cage layer).

2.2. Computational Methods

Molecular modeling and geometry optimization were performed using Avogadro2 (Version: 1.95.1). The force field for the optimization was MMFF94s using conjugate gradient as the optimization algorithm. Additional geometry optimization and energy calculations based on density functional theory (DFT) calculations were performed using the computational chemistry NWCHEM package [39]. The results were obtained using the B3LYP exchange correlation functional combined with Dunning's basis set (cc-pVDZ).

2.3. Sample Characterization

The Fourier transform infrared (FTIR) spectra of non-annealed and annealed PV4D4 thin films were recorded in transmission mode via an FTIR spectrometer (Bruker, Invenio-R, Billerica, MA, USA). The scan range was 400 cm^{-1} to 4000 cm^{-1} and the step width was 4 cm^{-1} step at 32 scans. Baseline correction was performed in graphing software (OriginLab, Origin Pro 2017).

The gas-sensing properties of both samples were calculated according to Equation (1), where a percentage-based ratio was obtained from G_{gas} and G_{air} [32]. The variable G is the conductance, which was calculated with a formula of one divided by the resistance of the sample in the air for G_{air} and in the same way for the G_{gas} conductance influenced by the applied gas.

$$S = \frac{G_{gas} - G_{air}}{G_{air}} \times 100\% \quad (1)$$

The gas response of the samples was measured by using a custom setup and protocol based on a previously described computer-controlled source-meter (Keithley 2400, Keithley Instruments, Cleveland, OH, USA) [40], while the sample was heated to different operating temperatures and under a constant gas flow to determine the results discussed below.

3. Results and Discussion

The fabricated hybrid sensors were investigated with regard to their chemical and gas-sensing properties.

3.1. Characterization of the Fabricated Sensors

We investigated the two different sample sets (ring and cage layers) by FTIR. First of all, the reaction mechanism of film formation is shown in Figure 2a.

The free-radical polymerization during the iCVD process leads to the formation of PV4D4 thin films via free-radical polymerization from the vapor phase, as illustrated in Figure 2a. The FTIR result of the deposited PV4D4 films is presented in Figure 2b. The as-deposited PV4D4 film (ring layer), represented by the orange line in Figure 2b, shows the characteristic band for the cyclotetrasiloxane rings, as also reported in previous studies [4,32]. Successful polymerization is indicated by the absence of bands above 3000 cm^{-1} , which represent the C-H stretching of sp^2 -hybridized carbon, i.e., vinyl groups. A change in the FTIR spectrum can be observed after the annealing of the PV4D4 thin films

(ring layer) at 450 °C, represented by the magenta line in Figure 2b. The cyclotetrasiloxane rings in the film appear to be transformed into silsesquioxane structures, as also reported by Trujillo et al. [34]. The transformation is illustrated in Figure 2c. The formation of the silsesquioxane cage structures occurs in the presence of oxygen and heat. The graphs in Figure 2d,e show a more detailed view of the areas that changed significantly after the heating step. The band for the cyclotetrasiloxane ring located around 1050 cm^{-1} for the as-deposited film (Figure 2d) transforms into a band for the silsesquioxane structures around 1110 cm^{-1} and a suboxide structure, as also observed in the literature [34]. A similar development is observed in the Si-C-related bands near 800 cm^{-1} (Figure 2e). The observed formation of the cage layer changes the free volume in the polymer film. This may provide alternative pathways for gas molecules compared to the ring layer (as-deposited PV4D4). In order to investigate the free volume and possible pathways for the gas molecules, geometry optimizations are performed using force field optimization and DFT. Figure 3a shows an octamethylcyclotetrasiloxane molecule representing the cyclotetrasiloxane rings in the as-deposited PV4D4. Figure 3b depicts the associated silsesquioxane cage, which forms after the annealing step.

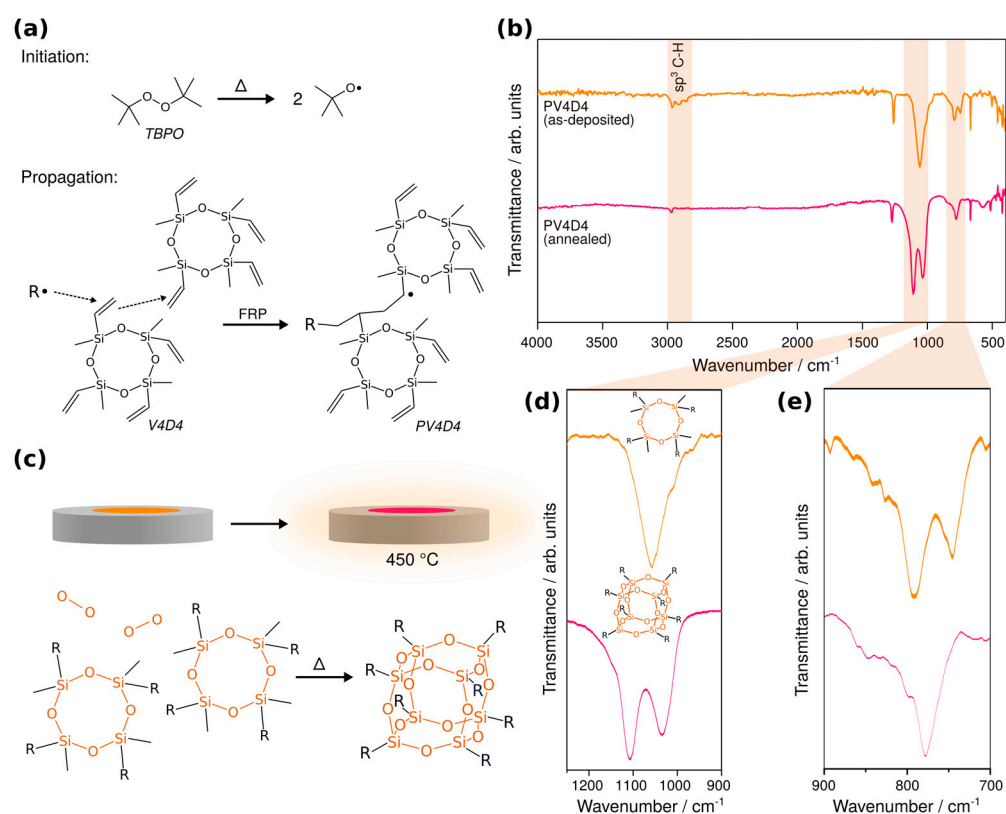


Figure 2. Investigation of PV4D4 film transformation into silsesquioxane cage structures. (a) Illustration of the free-radical polymerization reaction mechanism during iCVD PV4D4 film growth. (b) FTIR spectra of as-deposited PV4D4 thin films (orange line) and annealed PV4D4 thin films (magenta line) reveal different peaks. (c) Illustration of the cyclotetrasiloxane ring transformation into silsesquioxane cage structures during annealing. (d) Detailed view of the siloxane-related bands around 1050 cm^{-1} and (e) the observed band modification around 800 cm^{-1} .

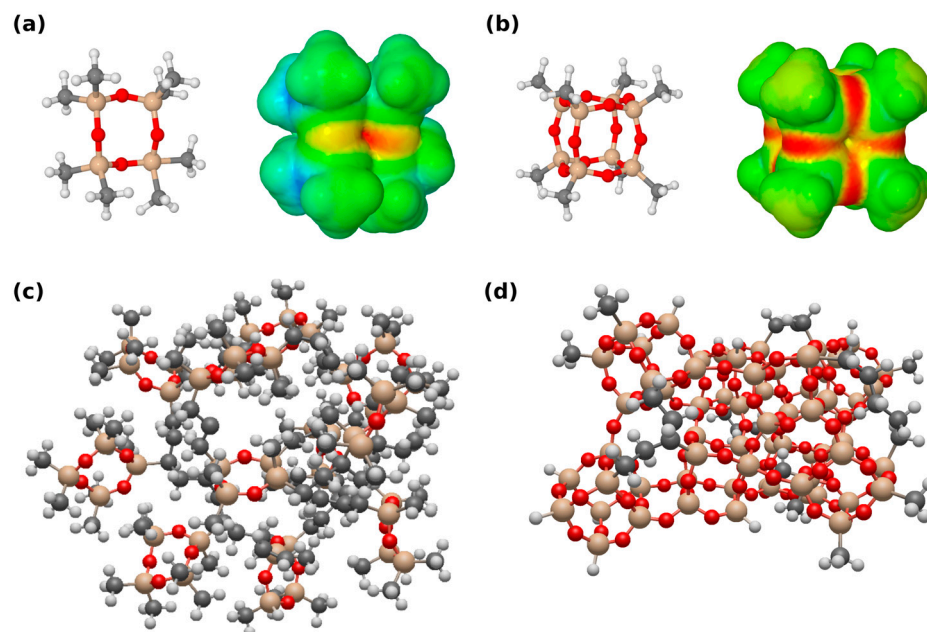


Figure 3. Computational view of the fabricated siloxane-based iCVD coatings. Red = oxygen, brown = silicon, Black = carbon, white = Hydrogen (a) Octamethylcyclotetrasiloxane molecule and its associated electrostatic potential map, representing PV4D4. (b) Silsesquioxane cage and its associated electrostatic potential map, representing annealed PV4D4. (c) Force field geometry-optimized approximated network extract for as-deposited PV4D4 and (d) the interconnected silsesquioxane cages formed after the annealing.

The free electron pair might undergo an interaction with polar molecules with high dipole moments and block some of these molecules. The suggested connection of two cyclotetrasiloxane rings and four oxygen atoms to form a siloxane cage may lead to denser packing of the molecules. This is also illustrated in Figure 3c,d, which represent the as-deposited PV4D4 network and the silsesquioxane cage network, respectively. This is also demonstrated by a slight decrease in polymer film thickness after the transformation process. The denser network may block larger molecules, as well as polar molecules with large dipole moments, due to electrostatic interaction with the free electron pairs provided by the oxygen, as mentioned above. However, transport may also occur through the silsesquioxane regions. The cages provide a more 3D character to the film, because the gas molecules can enter the cages from multiple sides and channels are more likely formed, which may favor gas transport through the polymer film. The cyclo layer may also allow molecules to pass through, but due to the flatter 2D geometry of the rings, the alignment is more random. This may partially block or redirect the gas molecules during their path through the film and reduce the response of the sensor.

In order to investigate the surface of the sensors, scanning electron microscopy (SEM) images were recorded. Figure 4 shows images of TiO_2 films with a cage layer without AgPt NPs (Figure 4a) and with AgPt NPs (Figure 4b). Figure 4a shows that the TiO_2 films with a cage layer without AgPt NPs show a uniform granular morphology with interconnected grains that completely cover the glass substrate. Figure 4b shows a similar TiO_2 film with a cage layer but functionalized with AgPt NPs, in which a uniform distribution of NPs can be observed.

To check the influence of the cage layer on the measurements and to detect changes in the selectivity of the sensors, gas-sensing measurements were performed.

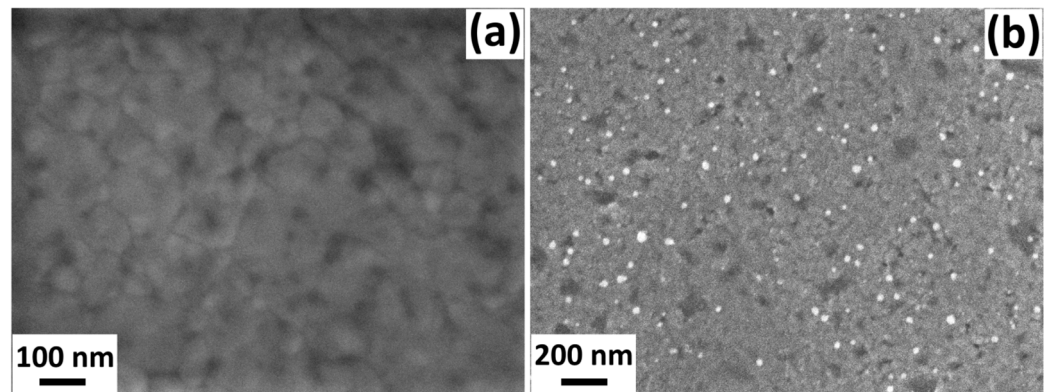


Figure 4. SEM images of TiO₂ films with cage layer: (a) without AgPt NPs and (b) with AgPt NPs.

3.2. Gas-Sensing Measurements and Evaluation

Figure 5 shows the measurement results for the response of the hybrid sensors with the a cyclo layer (Figure 5a) and a cage layer (Figure 5b) to different gases.

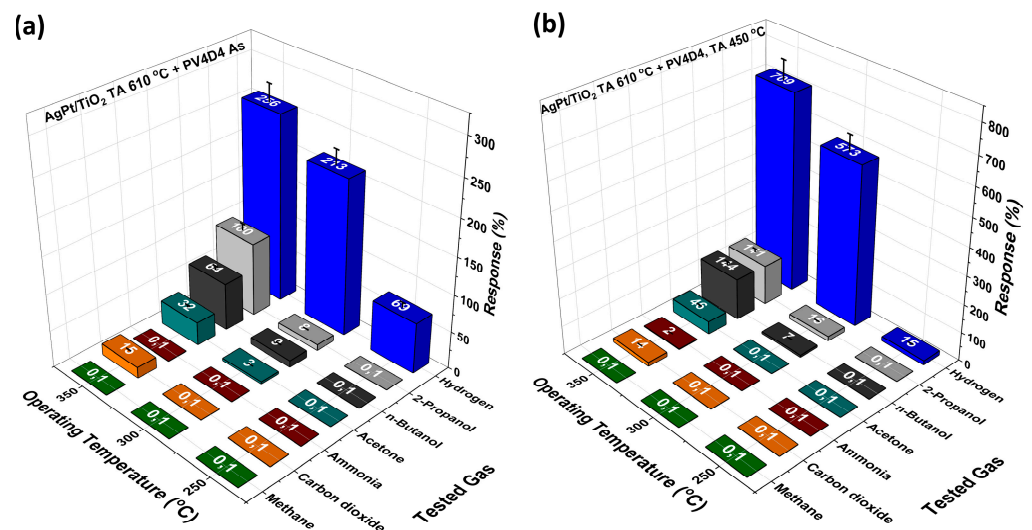


Figure 5. Gas responses of the hybrid sensors for different gases and operation temperatures. (a) These measurements were performed for a hybrid sensor with cyclo layer. (b) This plot shows the gas measurement results for hybrid sensors with a cage layer.

The gas response was measured for H₂, 2-propanol, butanol, acetone, ammonia (NH₃), carbon dioxide (CO₂) and methane (CH₄) at a concentration of 100 ppm. Figure 5a reveals that the hybrid sensor with a cyclo layer shows the highest response to H₂. A response of ~256% was obtained at an operating temperature of 350 °C. At 300 °C and 250 °C H₂ responses of ~213% and ~69%, respectively, were still obtained. At lower temperatures (<250 °C), the hybrid sensor with a cyclo layer no longer shows a response. In addition, at 350 °C, the sensor shows small response to 2-propanol, butanol, acetone and CO₂. The hybrid sensors with cage layer (Figure 5b) show similar selectivity to the same gases. However, the response to the gases is much higher. The response to H₂ is now ~709% at 350 °C and still ~573% at 300 °C. At 300 °C, the cage layer even shows a much higher response than the cyclo layer. Interestingly, the H₂ response almost vanishes at 250 °C, which may occur as a result of the formed cage structures of the polymer. At 250 °C, the molecular vibrations might be still too low to let molecules pass through, acting as a filter. A similar phenomenon was observed in a study [41] in which certain porous polymers filtered H₂, H₂O and CH₄ from benzene and o-xylene, which increased the selectivity. The response to other vapors is generally higher for the cage layer, which could be the result of better penetration of oxygen species at the surface. We expect the operating

temperature to be high, because at lower operating temperatures, relatively low sensitivity is expected. The gas molecules might not have enough thermal energy to react with the oxygen species adsorbed on the surface. Consequently, TiO₂-based gas sensors have an optimized operating temperature [42].

Dynamic response measurements for H₂ at a 300 °C operation temperature are shown in Figure 6a. The dynamic response to H₂ is measured at a concentration of 100 ppm. The highest response (~709%) was measured at 350 °C. The dynamic response is shown in Figure 6b. For Figure 6a, the first pulse shows a response time of $\tau_{res} \sim 26.96$ s from the start of gas introduction to the peak response and a recovery time $\tau_{rec} \sim 42.84$ s for full recovery to the initial signal. For the second pulse, values of $\tau_{res} \sim 32.15$ s and $\tau_{rec} \sim 35.40$ s are recorded, and for the third pulse, $\tau_{res} \sim 26.33$ s and $\tau_{rec} \sim 19.59$ s. In Figure 6b, the first pulse has response times of $\tau_{res} \sim 3.02$ s and $\tau_{rec} \sim 23.23$ s, while the second pulse has $\tau_{res} \sim 0.71$ s and $\tau_{rec} \sim 1.67$ s.

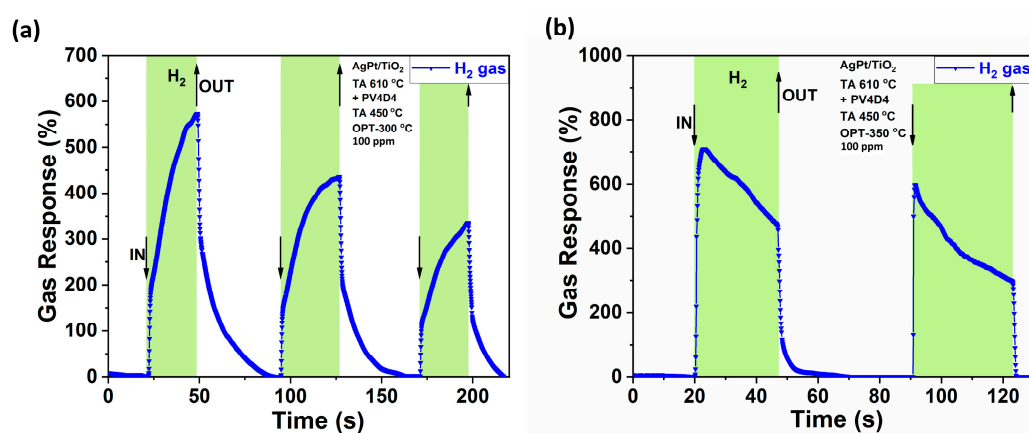
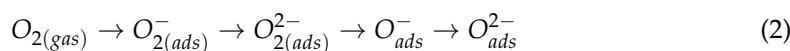


Figure 6. Dynamic response of the hybrid sensor with cage layer to H₂ molecules at (a) 300 °C operating temperature and (b) 350 °C operating temperature.

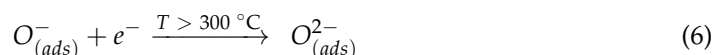
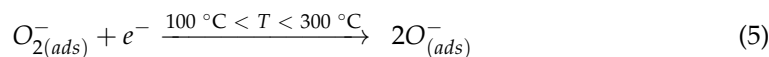
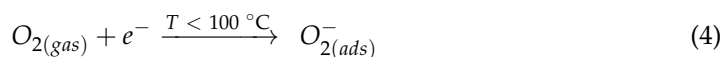
In addition to the response and dynamic response, the limit of detection (LOD) is an important parameter. A theoretical detection limit of ~1 ppm was estimated using the signal-to-noise ratio² formula, as reported by Dua et al. [43], used also in another similar study on gas sensors [44]. The obtained result is shown in Figure 7. Hydrogen of different concentrations (1 ppm, 5 ppm, 10 ppm, 50 ppm, 100 ppm, 500 ppm, 1000 ppm) was applied to the sample at two different temperatures: 300 °C and 350 °C. The tendencies are similar as both measurement lines look alike. A red line was fitted for each temperature to determine the theoretical value for the LOD.

In order to explain the results of the measurements, we first look at the gas-detection mechanism. It can be explained by the physico-chemical effects (electronic and chemical sensitization effects) that occur on the surface of the TiO₂ structures, taking into account the functionalization of the surface structures with Ag-Pt bimetallic NPs and the coating of the polymer layer. In order to obtain a general view of the species of reactive oxygen, which can be adsorbed on the surface of the structures, Anpo et al. made a classification for them [45]. According to this classification, the suprafacial class includes O_{ads}^- ; $O_{2\ ads}^-$; $O_{2\ ads}^{2-}$; and O_{ads}^{3-} , while the intrafacial class includes O_{surf}^- and O_{surf}^{2-} . Other species are distinguished as mixed interfacial (O_{ads}^- ; O_{ads}^-) and, as observed in nanoporous materials, clathrates (O_{cage}^- ; O_2^- ; $O_{2\ cage}^{2-}$; O_{cage}^{2-}) [45]. Via a series of consecutive reduction and dissociation steps, the formation of different reactive oxygen species may occur, like in the sequence proposed below:



However, there is a possibility that this basic scheme is not always rigorously followed, as there may be a change in the electron and proton affinities of the resultant oxygen

species. Thus, as stated in a paper with similar research [46] on gas-sensing mechanisms, the authors specified which species of oxygen reacted from their perspective. They show, as references for different operating temperatures, the following formulas [46]:



Besides all these, the Ag-Pt bimetallic NPs with which the surface of the TiO₂ structures was functionalized have an influence on the gas detection mechanism. Thus, the catalytic properties of bimetallic NPs are predominant in our case (the dominant effect is chemical sensitization) [37]. At higher operating temperatures, the selectivity towards H₂ gas changes, which can be explained by the polymer layer that covers the structures. The suggested sensing process is illustrated in Figure 8.

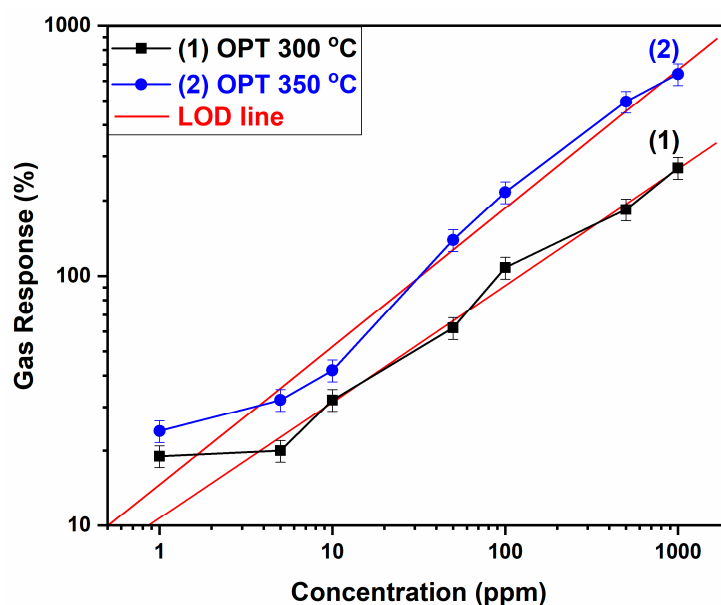


Figure 7. Limit-of-detection graph for H₂-sensing hybrid sensors at different concentrations at (1) 300 °C and (2) 350 °C operation temperatures.

Figure 8a,b represent a hybrid sensor with a cyclo layer and a hybrid sensor with a cage layer, respectively. Both are illustrated in air, and as observed in the results shown in Figure 5b, the denser network (Figure 3d) might block larger gas molecules, as well as polar molecules with large dipole moments, due to the electrostatic interaction with the free electron pairs provided by oxygen. At the same time, transport can also take place between more open silsesquioxane cages, as mentioned above, which allows for larger regions of free space and the formation of channels. The channels enable more efficient transport of the gas molecules through the layer, because the molecules can enter the cages from multiple sides. The observed significant increase in the gas response of the hybrid sensors with cage layers could thus be explained by the formation of channels/tunnels in the cage layer due to the presence of more interconnected silsesquioxane cage structures compared to the random aligned cyclotetrasiloxane rings present in the cyclo layer. The rings may partially block or redirect the gas molecules, which reduces the overall response

of the sensor. The more efficient alignment in the cage layer may enable an easier flow of H_2 molecules through it.

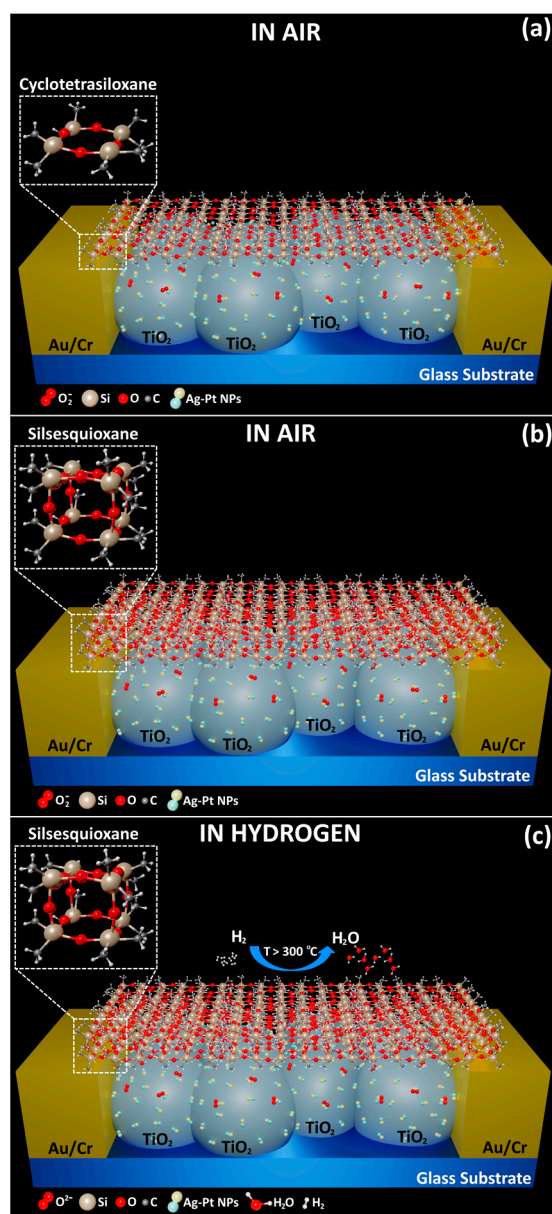
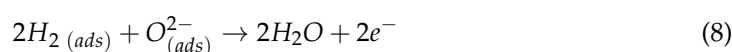


Figure 8. The proposed sensing mechanism of the hybrid gas sensors with (a) a cyclo layer (cyclotetrasiloxane polymer) in air; (b) a cage layer (silsesquioxane polymer) in air; and (c) a cage layer in hydrogen.

At high operating temperatures (Figure 8c), $O_{(ads)}^{2-}$ oxygen species are adsorbed on the surface of the structures, which interact with H_2 gas molecules. Due to the catalytic properties of the Ag-Pt NPs, a higher response occurs, a fact that is explained by the spillover effect and the oxidation of hydrogen molecules to the adsorbed oxygen species. In the case of H_2 gas detection, the oxygen species that is obtained on the surface is O^{2-} , because the operating temperature is 300 °C or higher, and the H_2 gas detection mechanism (Figure 8c) can finally be described according to the following relations:



With regard to applications, the effect of humidity when using cyclosiloxane-based polymers was investigated, and the results are shown in Figure S1 of the Supplementary Materials. In addition, there are also humidity-related studies presented in our previous work [31]. This study demonstrates that the hydrogen response at 350 °C is the same even at high relative humidity. Long-term stability is another important characteristic of a sensor. We show the long-term stability of one of our sensors in the Supplementary Materials (Figure S2). In general, the use of materials that have stable properties over time is essential. A combination of aluminum oxide and zinc oxide (Al₂O₃/ZnO) has been shown to provide time-stable sensors for the detection of 2-Propanol vapors and those in batteries [47,48]. The use of titanium oxide was also shown to provide time-stable ethanol sensors [40]. For its comparison to other gas-sensing materials in this category, we present the data in Table 1. It shows that the results obtained in this study are promising. The optimal operating temperature for the highest response is 350 °C. Thus, MOX sensors functionalized with an additional ultrathin polymer film, i.e., hybrid gas sensors, provide new pathways in sensor development.

Table 1. Comparison of different sensors' responses to H₂.

No.	Material	Functionalization	Polymer	Operating Temperature	H ₂ Response (%)	Ref.
1.	TiO ₂	-	-	250 °C	600	[30]
2.	TiO ₂	-	-	300 °C	650	[10]
3.	NiO	-	-	250 °C	97.2	[49]
4.	TiO ₂ /CuO/Cu ₂ O	Pd	-	250 °C	543	[35]
5.	ZnO:Ag	AgPt	-	250 °C	~400 *	[37]
6.	TiO ₂	Au	-	325 °C	70	[30]
7.	CNT	Pd/Pt	-	RT	520	[50]
8.	TiO ₂	-	PV4D4	300 °C	100	[4]
9.	SnO ₂	-	Teflon AF-2400	230 °C	75	[51]
10.	TiO ₂	AgPt	PV4D4	350 °C	~709.07	This work

*: estimated from graphs.

4. Conclusions

In summary, this study assessed the performance of two sets of hybrid gas sensors. The first contained a cyclotetrasiloxane-containing polymer top layer (cyclo layer), and the second sample set contained a polymer top layer with silsesquioxane cage structures (cage layer). The cyclo layer was transformed into a cage layer by thermal annealing at 450 °C in ambient air, as confirmed by FTIR measurements. Our results showed that the cage layer enabled a significantly increased response to H₂ (~256% vs. ~709%). We suggested that additional pathways/channels for the gas molecules were formed in the polymer layer after the transformation from the cyclo to the cage layer. In addition, we provided an approach to describe the sensing mechanism after the gas molecules have passed the polymer layer. These results provide new pathways for the development of hybrid gas sensors for the medical field. The precise tuning of the polymer top layer enables the tailoring of sensor properties, i.e., selectivity and sensitivity. These sensors could have further applications in the field of biomarker detection in human breath, where H₂ indicates gastrointestinal diseases. Additional experiments are required to find the reason for the blocking of H₂ at temperatures <250 °C and the influence of different materials for the top layer to further tune the selectivity and sensitivity of hybrid gas sensors.

Supplementary Materials: The following supporting information can be downloaded at: <https://www.mdpi.com/article/10.3390/chemosensors12050076/s1>, Table S1. Gas response data in % for Figure 5a; Table S2. Gas response data in % for Figure 5b; Figure S1. (a) Comparison of hybrid sensor responses at different relative humidity levels; (b) dynamic response of the cage layer hybrid sensor to H₂ molecules at a 350 °C operating temperature and 50% relative humidity; Figure S2. Long-term stability of one of the sensors applied in this study.

Author Contributions: Conceptualization, O.L. and S.S.; methodology, O.L., M.B., R.A. and S.S.; software, S.S., M.B. and N.A.; validation, R.A., O.L., F.F., S.S. and T.S.; formal analysis, M.B., L.Z.; investigation, M.B., J.P., N.A., N.M., L.Z., O.L. and T.P.; resources, R.A. and F.F.; data curation, O.L. and T.S.; writing—original draft preparation, M.B., S.S., J.P., N.A. and O.L.; writing—review and editing, O.L., R.A. and T.P.; visualization, N.A., M.B., N.M. and S.S.; supervision, T.S., O.L. and F.F.; project administration, O.L. and F.F.; funding acquisition, F.F. and R.A. All authors have read and agreed to the published version of the manuscript.

Funding: This work was funded by the German Research Foundation (DFG—Deutsche Forschungsgemeinschaft) under Project ID 434434223-SFB 1461, Project ID 286471992-SFB 1261 project A2, AD 183/16-1 and AD 183/18-1. Furthermore, this work was partially supported by the State Program LIFETECH No. 020404 and 020401 at the Technical University of Moldova. We acknowledge funding from the SulfurSilicon Batteries (SuSiBaBy) Project of the EUSH and EFRE in SH (LPW-E/3.1.1/1801).

Institutional Review Board Statement: Not applicable.

Informed Consent Statement: Not applicable.

Data Availability Statement: All data contained within the article and the supplementary materials.

Acknowledgments: O.L. gratefully acknowledges the CNRS Council for his support at IRCP Chimie ParisTech, Paris. Last, but not least, the authors thank Rohit Gupta and Alexander Vahl for the deposition of the Ag-Pt nanoparticles.

Conflicts of Interest: The authors declare no conflicts of interest.

References

1. Pathak, A.K.; Swargiary, K.; Kongsawang, N.; Jitpratak, P.; Ajchareeyasontorn, N.; Udomkittivorakul, J.; Viphavakit, C. Recent Advances in Sensing Materials Targeting Clinical Volatile Organic Compound (VOC) Biomarkers: A Review. *Biosensors* **2023**, *13*, 114. [[CrossRef](#)] [[PubMed](#)]
2. Hajivand, P.; Carolus Jansen, J.; Pardo, E.; Armentano, D.; Mastropietro, T.F.; Azadmehr, A. Application of Metal-Organic Frameworks for Sensing of VOCs and Other Volatile Biomarkers. *Coord. Chem. Rev.* **2024**, *501*, 215558. [[CrossRef](#)]
3. Choi, Y.J.; Lee, M.J.; Byun, M.K.; Park, S.; Park, J.; Park, D.; Kim, S.-H.; Kim, Y.; Lim, S.Y.; Yoo, K.H.; et al. Roles of Inflammatory Biomarkers in Exhaled Breath Condensates in Respiratory Clinical Fields. *Tuberc. Respir. Dis.* **2024**, *87*, 65–79. [[CrossRef](#)] [[PubMed](#)]
4. Brinza, M.; Schröder, S.; Ababii, N.; Gronenberg, M.; Strunskus, T.; Pauporte, T.; Adelung, R.; Faupel, F.; Lupan, O. Two-in-One Sensor Based on PV4D4-Coated TiO₂ Films for Food Spoilage Detection and as a Breath Marker for Several Diseases. *Biosensors* **2023**, *13*, 538. [[CrossRef](#)] [[PubMed](#)]
5. Fu, L.; Xu, J.; Liu, Q.; Liu, C.; Fan, S.; Ramakrishna, S.; Tang, W. Gas Sensors Based on Co₃O₄/TiO₂ Core-Shell Nanofibers Prepared by Coaxial Electrospinning for Breath Marker Acetone Detection. *Ceram. Int.* **2024**, *50*, 3443–3452. [[CrossRef](#)]
6. Aasi, A.; Aghaei, S.M.; Panchapakesan, B. Noble Metal (Pt or Pd)-Decorated Atomically Thin MoS₂ as a Promising Material for Sensing Colorectal Cancer Biomarkers through Exhaled Breath. *Int. J. Comput. Mater. Sci. Eng.* **2023**, *13*, 2350014. [[CrossRef](#)]
7. Yu, Y.-H.; Lin, X.-Y.; Teng, K.-L.; Hu, C.-C.; Wang, W.-Y.; Hung, Y.-H.; Tseng, H.-Y.; Luo, K.-H.; Yeh, J.-M.; Lu, K.-L.; et al. Semiconductive (Cu-S)n Metal-Organic Frameworks Hybrid Polyaniline Nanocomposites as Hydrogen Sulfide Gas Sensor. *Surf. Interfaces* **2024**, *44*, 103698. [[CrossRef](#)]
8. Kim, S.; Song, Y.; Ahn, H.-J.; Jeong, H.-M.; Yoo, B.U.; Lee, J.-Y. Ultrafast Response/Recovery and High Sensitivity of a Hydrogen Gas Sensor at Room Temperature Based on Electrochemically Deposited Sb₂Te₃/Polystyrene Composite Film. *Int. J. Hydrogen Energy* **2024**, *50*, 959–972. [[CrossRef](#)]
9. Wu, G.; Du, H.; Pakravan, K.; Kim, W.; Cha, Y.L.; Beidaghi, M.; Zhang, X.; Pan, X.; Kim, D.-J. Wearable Room-Temperature Ethanol Sensor Based on Ti₃C₂T_x/Polypyrrole Functionalized Face Mask for Drunk Driving Monitoring. *Carbon N. Y.* **2024**, *216*, 118565. [[CrossRef](#)]
10. Ababii, N.; Hoppe, M.; Shree, S.; Vahl, A.; Ulfa, M.; Pauporté, T.; Viana, B.; Cretu, V.; Magariu, N.; Postica, V.; et al. Effect of Noble Metal Functionalization and Film Thickness on Sensing Properties of Sprayed TiO₂ Ultra-Thin Films. *Sens. Actuators A Phys.* **2019**, *293*, 242–258. [[CrossRef](#)]
11. Dutta, T.; Noushin, T.; Tabassum, S.; Mishra, S.K. Road Map of Semiconductor Metal-Oxide-Based Sensors: A Review. *Sensors* **2023**, *23*, 6849. [[CrossRef](#)] [[PubMed](#)]
12. Wang, R.; Cheng, B.; Ou, W. Intrinsic and Ag-Doped Graphdiyne as a Two-Dimensional Material Gas Sensing Detector for the Detection of SF₆ Decomposition Products. *Appl. Surf. Sci.* **2023**, *608*, 155276. [[CrossRef](#)]
13. Bi, Y.; Zhao, Y.; Meng, X.; Cong, H.; Gao, W. Synthesis of Ag-Pt Bimetallic Functionalized α -Fe₂O₃ for Rapid Triethylamine Detection at Low Temperature. *Chem. Phys. Lett.* **2023**, *813*, 140301. [[CrossRef](#)]
14. Borowik, P.; Adamowicz, L.; Tarakowski, R.; Siwek, K.; Grzywacz, T. Odor Detection Using an E-Nose With a Reduced Sensor Array. *Sensors* **2020**, *20*, 3542. [[CrossRef](#)] [[PubMed](#)]

15. Bhangare, B.; Sinju, K.R.; Ramgir, N.S.; Gosavi, S.; Debnath, A.K. Noble Metal Sensitized SnO₂/RGO Nanohybrids as Chemiresistive E-Nose for H₂, H₂S and NO₂ Detection. *Mater. Sci. Semicond. Process.* **2022**, *147*, 106706. [[CrossRef](#)]
16. Zhang, W.; Wang, L.; Chen, J.; Bi, X.; Chen, C.; Zhang, J.; Hans, V. A Novel Gas Recognition and Concentration Estimation Model for an Artificial Olfactory System With a Gas Sensor Array. *IEEE Sens. J.* **2021**, *21*, 18459–18468. [[CrossRef](#)]
17. Lekha, S.; Suchetha, M. Recent Advancements and Future Prospects on E-Nose Sensors Technology and Machine Learning Approaches for Non-Invasive Diabetes Diagnosis: A Review. *IEEE Rev. Biomed. Eng.* **2021**, *14*, 127–138. [[CrossRef](#)] [[PubMed](#)]
18. Moshayedi, A.J.; Khan, A.S.; Shuxin, Y.; Kuan, G.; Hu, J.; Soleimani, M.; Razi, A. E-Nose Design and Structures from Statistical Analysis to Application in Robotic: A Compressive Review. *EAI Endorsed Trans. AI Robot.* **2023**, *2*, 1–20. [[CrossRef](#)]
19. Ochoa-Muñoz, Y.H.; Mejía de Gutiérrez, R.; Rodríguez-Páez, J.E. Metal Oxide Gas Sensors to Study Acetone Detection Considering Their Potential in the Diagnosis of Diabetes: A Review. *Molecules* **2023**, *28*, 1150. [[CrossRef](#)]
20. Ong, W.L.; Zhang, C.; Ho, G.W. Ammonia Plasma Modification towards a Rapid and Low Temperature Approach for Tuning Electrical Conductivity of ZnO Nanowires on Flexible Substrates. *Nanoscale* **2011**, *3*, 4206–4214. [[CrossRef](#)]
21. Rashid, T.-R.; Phan, D.-T.; Chung, G.-S. Effect of Ga-Modified Layer on Flexible Hydrogen Sensor Using ZnO Nanorods Decorated by Pd Catalysts. *Sens. Actuators B Chem.* **2014**, *193*, 869–876. [[CrossRef](#)]
22. Rashid, T.-R.; Phan, D.-T.; Chung, G.-S. A Flexible Hydrogen Sensor Based on Pd Nanoparticles Decorated ZnO Nanorods Grown on Polyimide Tape. *Sens. Actuators B Chem.* **2013**, *185*, 777–784. [[CrossRef](#)]
23. Mohammad, S.M.; Hassan, Z.; Talib, R.A.; Ahmed, N.M.; Al-Azawi, M.A.; Abd-Alghafour, N.M.; Chin, C.W.; Al-Hardan, N.H. Fabrication of a Highly Flexible Low-Cost H₂ Gas Sensor Using ZnO Nanorods Grown on an Ultra-Thin Nylon Substrate. *J. Mater. Sci. Mater. Electron.* **2016**, *27*, 9461–9469. [[CrossRef](#)]
24. Wang, P.; Shao, Z.; Ulfa, M.; Pauporté, T. Insights into the Hole Blocking Layer Effect on the Perovskite Solar Cell Performance and Impedance Response. *J. Phys. Chem. C* **2017**, *121*, 9131–9141. [[CrossRef](#)]
25. Punetha, D.; Kar, M.; Pandey, S.K. A New Type Low-Cost, Flexible and Wearable Tertiary Nanocomposite Sensor for Room Temperature Hydrogen Gas Sensing. *Sci. Rep.* **2020**, *10*, 2151. [[CrossRef](#)] [[PubMed](#)]
26. Ou, L.-X.; Liu, M.-Y.; Zhu, L.-Y.; Zhang, D.W.; Lu, H.-L. Recent Progress on Flexible Room-Temperature Gas Sensors Based on Metal Oxide Semiconductor. *Nano-Micro Lett.* **2022**, *14*, 206. [[CrossRef](#)] [[PubMed](#)]
27. Ma, Y.; Liang, T.; Qiao, S.; Liu, X.; Lang, Z. Highly Sensitive and Fast Hydrogen Detection Based on Light-Induced Thermoelastic Spectroscopy. *Ultrafast Sci.* **2023**, *3*, 24. [[CrossRef](#)]
28. Shin, W. Medical Applications of Breath Hydrogen Measurements. *Anal. Bioanal. Chem.* **2014**, *406*, 3931–3939. [[CrossRef](#)] [[PubMed](#)]
29. Korovljević, D.; Ostojic, J.; Todorovic, N.; Ostojic, S. Molecular Hydrogen Modulates Brain Glutamate/GABA-Glutamine Cycle in Overweight Humans. *Arch. Med. Sci.* **2023**, *19*, 1151–1153. [[CrossRef](#)]
30. Lupan, O.; Postica, V.; Ababii, N.; Reimer, T.; Shree, S.; Hoppe, M.; Polonskyi, O.; Sontea, V.; Chemnitz, S.; Faupel, F.; et al. Ultra-Thin TiO₂ Films by Atomic Layer Deposition and Surface Functionalization with Au Nanodots for Sensing Applications. *Mater. Sci. Semicond. Process.* **2018**, *87*, 44. [[CrossRef](#)]
31. Schröder, S.; Ababii, N.; Lupan, O.; Drewes, J.; Magariu, N.; Krüger, H.; Strunskus, T.; Adlung, R.; Hansen, S.; Faupel, F. Sensing Performance of CuO/Cu₂O/ZnO:Fe Heterostructure Coated with Thermally Stable Ultrathin Hydrophobic PV₃D₃ Polymer Layer for Battery Application. *Mater. Today Chem.* **2022**, *23*, 100642. [[CrossRef](#)]
32. Schröder, S.; Ababii, N.; Brînză, M.; Magariu, N.; Zimoch, L.; Bodduluri, M.T.; Strunskus, T.; Adlung, R.; Faupel, F.; Lupan, O. Tuning the Selectivity of Metal Oxide Gas Sensors with Vapor Phase Deposited Ultrathin Polymer Thin Films. *Polymers* **2023**, *15*, 524. [[CrossRef](#)] [[PubMed](#)]
33. Tenhaeff, W.E.; Gleason, K.K. Initiated and Oxidative Chemical Vapor Deposition of Polymeric Thin Films: ICVD and OCVD. *Adv. Funct. Mater.* **2008**, *18*, 979–992. [[CrossRef](#)]
34. Trujillo, N.J.; Wu, Q.; Gleason, K.K. Ultralow Dielectric Constant Tetravinyltetramethylcyclotetrasiloxane Films Deposited by Initiated Chemical Vapor Deposition (ICVD). *Adv. Funct. Mater.* **2010**, *20*, 607–616. [[CrossRef](#)]
35. Lupan, O.; Ababii, N.; Santos-Carballal, D.; Terasa, M.-I.; Magariu, N.; Zappa, D.; Comini, E.; Pauporté, T.; Siebert, L.; Faupel, F.; et al. Tailoring the Selectivity of Ultralow-Power Heterojunction Gas Sensors by Noble Metal Nanoparticle Functionalization. *Nano Energy* **2021**, *88*, 106241. [[CrossRef](#)]
36. Vahl, A.; Strobel, J.; Reichstein, W.; Polonskyi, O.; Strunskus, T.; Kienle, L.; Faupel, F. Single Target Sputter Deposition of Alloy Nanoparticles with Adjustable Composition via a Gas Aggregation Cluster Source. *Nanotechnology* **2017**, *28*, 175703. [[CrossRef](#)]
37. Vahl, A.; Lupan, O.; Santos-Carballal, D.; Postica, V.; Hansen, S.; Cavers, H.; Wolff, N.; Terasa, M.-I.; Hoppe, M.; Cadi-Essadek, A.; et al. Surface Functionalization of ZnO:Ag Columnar Thin Films with AgAu and AgPt Bimetallic Alloy Nanoparticles as an Efficient Pathway for Highly Sensitive Gas Discrimination and Early Hazard Detection in Batteries. *J. Mater. Chem. A* **2020**, *8*, 16246. [[CrossRef](#)]
38. Burk, M.H.; Schröder, S.; Moormann, W.; Langbehn, D.; Strunskus, T.; Rehders, S.; Herges, R.; Faupel, F. Fabrication of Diazocine-Based Photochromic Organic Thin Films via Initiated Chemical Vapor Deposition. *Macromolecules* **2020**, *53*, 1164–1170. [[CrossRef](#)]
39. Aprà, E.; Bylaska, E.J.; de Jong, W.A.; Govind, N.; Kowalski, K.; Straatsma, T.P.; Valiev, M.; van Dam, H.J.J.; Alexeev, Y.; Anchell, J.; et al. NWChem: Past, Present, and Future. *J. Chem. Phys.* **2020**, *152*, 184102. [[CrossRef](#)]

40. Lupan, O.; Santos-Carballal, D.; Ababii, N.; Magariu, N.; Hansen, S.; Vahl, A.; Zimoch, L.; Hoppe, M.; Pauporté, T.; Galstyan, V.; et al. TiO₂/Cu₂O/CuO Multi-Nanolayers as Sensors for H₂ and Volatile Organic Compounds: An Experimental and Theoretical Investigation. *ACS Appl. Mater. Interfaces* **2021**, *13*, 32363. [[CrossRef](#)]
41. van den Broek, J.; Weber, I.C.; Güntner, A.T.; Pratsinis, S.E. Highly Selective Gas Sensing Enabled by Filters. *Mater. Horiz.* **2021**, *8*, 661–684. [[CrossRef](#)] [[PubMed](#)]
42. Shooshtari, M.; Salehi, A.; Vollebregt, S. Effect of Temperature and Humidity on the Sensing Performance of TiO₂ Nanowire-Based Ethanol Vapor Sensors. *Nanotechnology* **2021**, *32*, 325501. [[CrossRef](#)] [[PubMed](#)]
43. Dua, V.; Surwade, S.P.; Ammu, S.; Agnihotra, S.R.; Jain, S.; Roberts, K.E.; Park, S.; Ruoff, R.S.; Manohar, S.K. All-Organic Vapor Sensor Using Inkjet-Printed Reduced Graphene Oxide. *Angew. Chem. Int. Ed.* **2010**, *49*, 2154–2157. [[CrossRef](#)] [[PubMed](#)]
44. Lupan, O.; Postica, V.; Pauporté, T.; Viana, B.; Terasa, M.-I.; Adelung, R. Room Temperature Gas Nanosensors Based on Individual and Multiple Networked Au-Modified ZnO Nanowires. *Sens. Actuators B Chem.* **2019**, *299*, 126977. [[CrossRef](#)]
45. Anpo, M.; Costentin, G.; Giamello, E.; Lauron-Pernot, H.; Sojka, Z. Characterisation and Reactivity of Oxygen Species at the Surface of Metal Oxides. *J. Catal.* **2021**, *393*, 259–280. [[CrossRef](#)]
46. Wang, B.; Zeng, Q.; Chen, S.; Yue, T.; Han, B.; Feng, W.; Yang, D. Preparation and Gas Sensing Performance of Hierarchical Porous ZnO-Based Materials with Sunflower Rods as a Biological Template. *Chem. Res. Chin. Univ.* **2019**, *35*, 755–761. [[CrossRef](#)]
47. Lupan, O.; Santos-Carballal, D.; Magariu, N.; Mishra, A.K.; Ababii, N.; Krüger, H.; Wolff, N.; Vahl, A.; Bodduluri, M.T.; Kohlmann, N.; et al. Al₂O₃/ZnO Heterostructure-Based Sensors for Volatile Organic Compounds in Safety Applications. *ACS Appl. Mater. Interfaces* **2022**, *14*, 29331–29344. [[CrossRef](#)] [[PubMed](#)]
48. Santos-Carballal, D.; Lupan, O.; Magariu, N.; Ababii, N.; Krüger, H.; Bodduluri, M.T.; de Leeuw, N.H.; Hansen, S.; Adelung, R. Al₂O₃/ZnO Composite-Based Sensors for Battery Safety Applications: An Experimental and Theoretical Investigation. *Nano Energy* **2023**, *109*, 108301. [[CrossRef](#)]
49. Pai, S.H.S.; Mondal, A.; Barathy T, R.; Ajitha, B.; Samuel E, J.J.; Reddy, Y.A.K. Effect of Calcination Temperature on NiO for Hydrogen Gas Sensor Performance. *Int. J. Hydrogen Energy* **2024**, *50*, 928–941. [[CrossRef](#)]
50. Gamboa, A.; Fernandes, E.C. Resistive Hydrogen Sensors Based on Carbon Nanotubes: A Review. *Sens. Actuators A Phys.* **2024**, *366*, 115013. [[CrossRef](#)]
51. Tan, Y.; Du, B.; Liang, C.; Guo, X.; Zheng, H.; Liu, P.; Yang, X.; Li, S.; Jin, B.; Sun, J. Improving Anti-Humidity Property of a SnO₂-Based Chemiresistive Hydrogen Sensor by a Breathable and Hydrophobic Fluoropolymer Coating. *Langmuir* **2022**, *38*, 13833–13840. [[CrossRef](#)] [[PubMed](#)]

Disclaimer/Publisher's Note: The statements, opinions and data contained in all publications are solely those of the individual author(s) and contributor(s) and not of MDPI and/or the editor(s). MDPI and/or the editor(s) disclaim responsibility for any injury to people or property resulting from any ideas, methods, instructions or products referred to in the content.